

# Lawrence Berkeley National Laboratory

## Materials Sciences

### Title

High Defect Tolerance in Lead Halide Perovskite CsPbBr<sub>3</sub>

### Permalink

<https://escholarship.org/uc/item/38j557sc>

### Journal

The Journal of Physical Chemistry Letters, 8(2)

### ISSN

1948-7185

### Authors

Kang, Jun  
Wang, Lin-Wang

### Publication Date

2017-01-19

### DOI

10.1021/acs.jpcllett.6b02800

Peer reviewed

# High Defect Tolerance in Lead Halide Perovskite



Jun Kang and Lin-Wang Wang\*

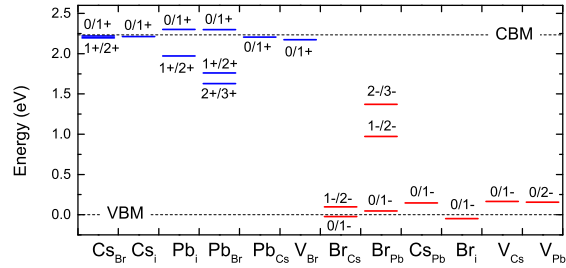
*Materials Sciences Division, Lawrence Berkeley National Laboratory, Berkeley, California  
94720, United States*

E-mail: [lwwang@lbl.gov](mailto:lwwang@lbl.gov)

## Abstract

The formation energies and charge transition levels of intrinsic point defects in lead halide perovskite CsPbBr<sub>3</sub> are studied from first-principles calculations. It is shown that the formation energy of dominant defect under Br-rich growth condition is much lower than that under moderate or Br-poor conditions. Thus avoiding the Br-rich condition can help to reduce the defect concentration. Interestingly, CsPbBr<sub>3</sub> is found to be highly defect tolerant in terms of its electronic structure. Most of the intrinsic defects induce shallow transition levels. Only a few defects with high formation energies can create deep transition levels. Therefore, CsPbBr<sub>3</sub> can maintain its good electronic quality despite the presence of defects. Such defect tolerance feature can be attributed to the lacking of bonding-antibonding interaction between the conduction bands and valence bands.

Table of Contents Graphic



Recently, lead halide perovskites (LHPs) have emerged as promising optoelectronic materials, and attracted an enormous amount of interest. They are medium-bandgap semiconductors and can be synthesized cost-effectively on large scales through simple solution-based processes.<sup>1-5</sup> One of the most impressive progresses is the rapidly increased power conversion efficiency of LHP-based solar cells, from a starting efficiency of  $\sim 4\%$ <sup>1</sup> to over  $20\%$ <sup>6,7</sup> within a few years. Besides photovoltaics, other applications of LHP, such as light-emitting diodes,<sup>8,9</sup> laser devices,<sup>10-12</sup> and photodectors,<sup>13,14</sup> have also been investigated. Although the organic-inorganic hybrid LHP like the MAPbI<sub>3</sub> has been studied extensively, the pure inorganic alternative, like the CsPbBr<sub>3</sub> has been recently found to possess most of the good properties of the hybrid LHP counterpart.<sup>15-17</sup> CsPbBr<sub>3</sub> has excellent luminescence properties, including extremely high quantum yield, narrow emission bandwidth without size-distribution, and suppressed photoluminescence (PL) blinking.<sup>18</sup> In addition, CsPbBr<sub>3</sub> also exhibits remarkably high carrier mobility and large diffusion length.<sup>19</sup> Moreover, CsPbBr<sub>3</sub> can be synthesized in various structures such as quantum dots, nanocubes, nanowires, nanoplates, and even two-dimensional (2D) layers with controllable sizes.<sup>3,5,17,20,21</sup> This allows one to modulate the quantum confinement effect in the nanostructures to achieve desired emitting wavelength. The 2D form of CsPbBr<sub>3</sub> is also a good candidate for ultrathin and flexible optoelectronics. All of these features make CsPbBr<sub>3</sub> a very promising semiconductor for future applications.

Defect properties, especially those of intrinsic point defects, of a semiconductor are always critical to its performance. The carrier mobility, lifetime, and recombination rate can be greatly affected by defects. Intrinsic defects also determine the doping limit. Therefore, a good understanding of the defect properties is important for the application of a material. Up to date, much theoretical work has been done on the defect properties in organic-inorganic hybrid LHP.<sup>22-26</sup> However, related studies on all-inorganic LHP are less reported. Although there are a few studies that include the defect properties of all-inorganic CsPbBr<sub>3</sub>,<sup>27,28</sup> a systematic theoretical investigation on the defect formation energy under different growth conditions, as well as the defect charge transition levels in CsPbBr<sub>3</sub>, is still missing.

In this work, we study the properties of intrinsic point defects in CsPbBr<sub>3</sub> from first-principles calculations. It is found that moderate or Br-poor growth condition can help to reduce the defect concentration in CsPbBr<sub>3</sub>. We also show that the dominant defects in CsPbBr<sub>3</sub> only introduce shallow transition levels, which usually are not carrier trapping centers, so CsPbBr<sub>3</sub> is a defect tolerant semiconductor. Our results can provide guidance for experimental synthesis to reduce the defect formation, and also provide insights for the high optoelectronic quality of this material despite the existence of point defects.

The formation energy  $\Delta H(\alpha, q)$  for a defect  $\alpha$  at charge state  $q$  is determined as:<sup>29,30</sup>

$$\Delta H(\alpha, q) = E(\alpha, q) - E(host) + \sum_i n_i(E_i + \mu_i) + q[E_{\text{VBM}}(host) + E_F + \Delta V]. \quad (1)$$

Here  $E(\alpha, q)$  is the total energy of the supercell containing the defect, and  $E(host)$  is the total energy of the same supercell with the absence of defect.  $E_{\text{VBM}}(host)$  is the valence band maximum (VBM) energy of the host material and  $E_F$  is the Fermi energy measured from VBM.  $\mu_i$  is the atomic chemical potential of constituent  $i$  referenced to the total energy  $E_i$  of its pure elemental solid or molecule (Cs metal, Pb metal, and Br<sub>2</sub> molecule for CsPbBr<sub>3</sub>).  $n_i$  is the number of atom  $i$ , and  $q$  is the number of electrons, transferred from the supercell to the reservoirs in forming the defect cell. For example, for a negatively charged Br<sub>Pb</sub> antisite (Br<sub>Pb</sub>, -1),  $n_{\text{Br}}=-1$ ,  $n_{\text{Pb}}=1$ , and  $q=-1$ . The potential alignment correction term  $\Delta V$  is added to align the VBM energy in systems with different charged states.<sup>31</sup> It is calculated by the energy shift of the 1  $s$  core-level energy of a Cs atom (which is far away from the defect site) between the neutral defect and charged cases. The defect charge transition energy level  $\epsilon(q/q')$  corresponds to the  $E_F$  at which the formation energy  $\Delta H(\alpha, q)=\Delta H(\alpha, q')$  for a defect  $\alpha$  with different charge state  $q$  and  $q'$ , i.e.,

$$\epsilon(q/q') = [E(\alpha, q) - E(\alpha, q') + (q - q')(E_{\text{VBM}} + \Delta V)]/(q' - q) \quad (2)$$

The calculations are carried out using the Vienna *ab initio* simulation package (VASP).<sup>32,33</sup>

The core-valence interaction is described by the projector augmented wave (PAW) method,<sup>34</sup> and the generalized gradient approximation of Perdew-Burke-Ernzerhof (GGA-PBE)<sup>35</sup> is used. The wavefunctions are expanded in a plane-wave basis set with a 400 eV cutoff. A  $3 \times 3 \times 2$  supercell containing 360 atoms is used for the defect calculations, and the Brillouin zone is sampled by the  $\Gamma$  point. Structure relaxation is stopped when the force on each atom is smaller than  $0.01 \text{ eV}/\text{\AA}$ . For the calculation of defect transition levels, more accurate description on the band structures is needed. It is well known that PBE gives reasonable total energy and structure, but severely underestimates the band gap. Moreover, Pb is a heavy element so the spin-orbital coupling (SOC) effect in  $\text{CsPbBr}_3$  can be significant. Therefore, we have used the the Heyd-Scuseria-Ernzerhof (HSE) hybrid functional<sup>36</sup> in combination with the SOC effect to calculate the defect transition levels. A  $2 \times 2 \times 2$  supercell and a 300 eV energy cutoff are used to reduce the computation cost of the HSE+SOC calculation. The mixing rate of the Hartree-Fock exchange potential is set to 0.43. With this setup, the calculated band gap of  $\text{CsPbBr}_3$  is 2.23 eV, which is in good agreement with the experimental value of 2.25 eV.<sup>37</sup> Phonon spectrum is calculated by the small displacement method using the PHON code.<sup>38</sup>

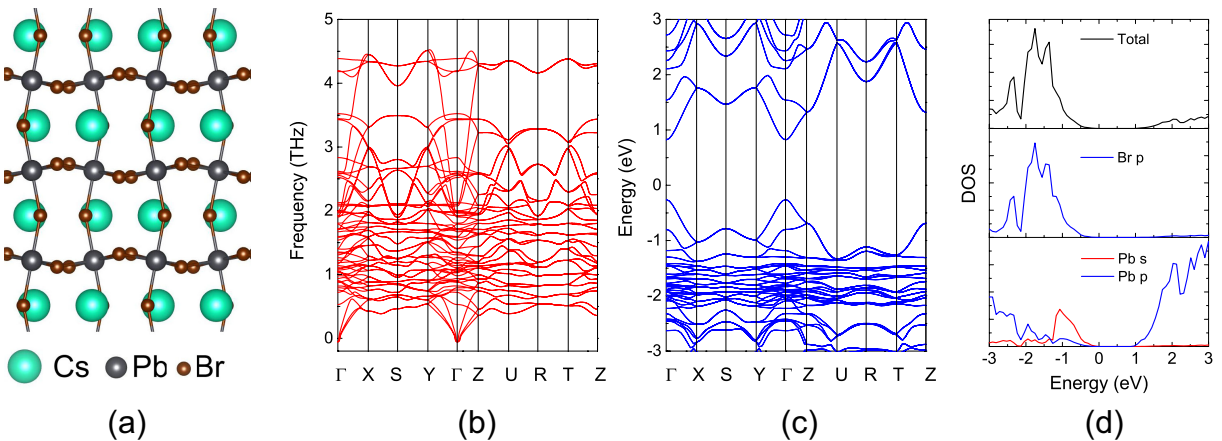


Figure 1: Lattice structure (a), phonon spectrum (b), PBE+SOC band structure (c), and density of states (d) for  $\text{CsPbBr}_3$  in the orthorhombic phase. Fermi level is set to 0 eV in (c) and (d).

At low temperature, the orthorhombic phase is most stable for  $\text{CsPbBr}_3$ .<sup>37</sup> Compared

with the cubic phase, the  $\text{PbBr}_6$  octahedra in the orthorhombic phase are slightly tilted, as seen in Fig. 1a. The optimized lattice constants are 8.23 Å, 8.50 Å and 11.89 Å. The phonon spectrum of  $\text{CsPbBr}_3$  is presented in Fig. 1b. There is no negative mode in the spectrum, indicating the stability of the optimized structure. The band structure of orthorhombic  $\text{CsPbBr}_3$  calculated by PBE+SOC is shown in Fig.1c. Both the valence band maximum (VBM) and the conduction band minimum (CBM) are located at the  $\Gamma$  point. The predicted band gap from PBE+SOC is 1.08 eV, which is severely underestimated compared with the experimental value of 2.25 eV.<sup>37</sup> On the other hand, our HSE+SOC calculations obtained a band gap of 2.23 eV, in good agreement with experiment. The density of states are given in Fig. 1d. The states around the band gap come from Br and Pb atoms, whereas Cs has no contribution. In the valence band, the Pb  $s$  and Br  $p$  states have strong hybridization, and their antibonding interaction leads to the formation of the upper valence band. On the other hand, the conduction band is formed through the coupling between the empty Pb  $p$  states. Due to the ionic character of  $\text{CsPbBr}_3$ , the antibonding interaction between the valence band and conduction band states are negligible, so the lower conduction bands have almost no contribution from Br atoms. Similar band characters have also been seen in hybrid LHP like  $\text{MAPbI}_3$  and  $\text{MaPbBr}_3$ .<sup>22,23</sup> Note that in many covalent-bond semiconductors (such as GaN), the valence bands and conduction bands originate from the bonding-antibonding orbital pairs. Our analysis indicates that the band structure character of  $\text{CsPbBr}_3$  is very different from covalent-bond semiconductors. Such feature can have important influences on the defect properties of  $\text{CsPbBr}_3$ , as we will discuss later.

From Eq. 1 we can see that, the defect formation energy depends on the chemical potentials of the constitute atoms. Under thermal equilibrium growth condition, there is a certain region of chemical potentials in which pure  $\text{CsPbBr}_3$  is stable, and the range of atomic chemical potentials is thus thermodynamically limited. In Eq. 1, the chemical potential  $\mu_i$  is referenced to Cs metal, Pb metal or  $\text{Br}_2$  molecule. To avoid the formation of these elementary substances, all  $\mu_i$  should be smaller than 0. Besides, more attention should be paid to the

Br case. Using an ideal gas model,  $\mu_{\text{Br}}$  (relative to the  $\text{Br}_2$  molecule ground state energy) can be expressed by the function of pressure  $P$  and temperature  $T$  as:<sup>39</sup>

$$\mu_{\text{Br}} = [H_0 + c_p(T - T_0) - TS_0 + Tc_p \ln(T/T_0) + k_B T \ln(P/P_0)]/2, \quad (3)$$

where  $k_B$  is the Boltzmann constant, and  $c_p=3.5 k_B$  is the constant pressure heat capacity for ideal gas of diatomic molecules.  $T_0$  and  $P_0$  are the temperature and pressure, respectively, at a reference state.  $H_0$  and  $S_0$  are the enthalpy and entropy differences, respectively, between the states at  $(T_0, P_0)$  and at 0 K.  $c_p(T - T_0)$  and  $Tc_p \ln(T/T_0)$  take account for the temperature variations of enthalpy and entropy, respectively, and  $k_B T \ln(P/P_0)$  is the pressure variation of the chemical potential. For  $\text{Br}_2$  gas under ambient conditions (300 K and 1 atm),  $H_0=9719$  J/mol, and  $S_0=245$  J/mol/K.<sup>40</sup> According to this relationship,  $\mu_{\text{Br}}=0$  is unrealistic since it can only be realized by some extreme conditions, *e.g.* when  $T \rightarrow 0$  K or  $P = 5 \times 10^{10}$  atm at  $T = 300$  K. Under ambient conditions,  $\mu_{\text{Br}}$  is -0.32 eV. This could be a more reasonable upper boundary for the chemical potential of Br. Moreover, equilibrium growth also requires that the chemical potentials should satisfy

$$\mu_{\text{Cs}} + \mu_{\text{Pb}} + 3\mu_{\text{Br}} = \Delta H(\text{CsPbBr}_3) = -7.09 \text{ eV},$$

where  $\Delta H(\text{CsPbBr}_3)$  is the formation energy of  $\text{CsPbBr}_3$ . Lastly, to avoid the formation of secondary phases such as  $\text{CsBr}$  and  $\text{PbBr}_2$ , the following limits should be applied:

$$\mu_{\text{Cs}} + \mu_{\text{Br}} < \Delta H(\text{CsBr}) = -3.34 \text{ eV},$$

$$\mu_{\text{Pb}} + 2\mu_{\text{Br}} < \Delta H(\text{PbBr}_2) = -3.09 \text{ eV},$$

where  $\Delta H(\text{CsBr})$  and  $\Delta H(\text{PbBr}_2)$  are the formation energies of  $\text{CsBr}$  and  $\text{PbBr}_2$ , respectively. With all of these limitations considered, the available equilibrium chemical potential region for  $\text{CsPbBr}_3$  is plotted in Fig. 2. The region is quite narrow. This can be understood by the low dissociation energy (0.25 eV according to our calculation) to decompose

CsPbBr<sub>3</sub> into CsBr and PbBr<sub>2</sub>. Nevertheless, inorganic CsPbBr<sub>3</sub> is more stable than the hybrid perovskite MAPbBr<sub>3</sub> whose dissociation energy is only 0.19 eV.<sup>23</sup>

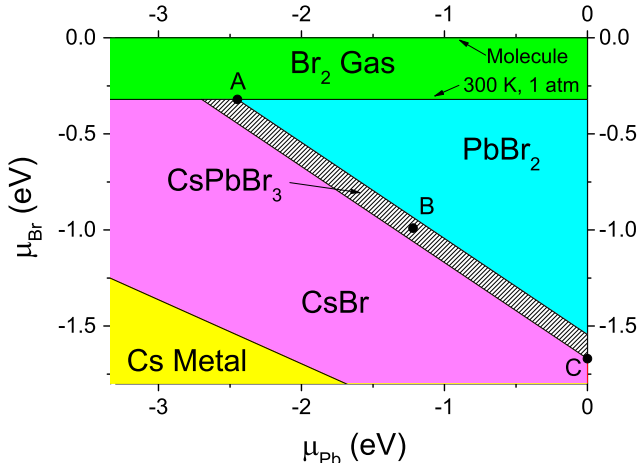


Figure 2: Stability regions of different compounds against Br and Pb chemical potentials.  $\mu_{\text{Br}} = 0$  corresponds to an isolated Br<sub>2</sub> molecule, whereas  $\mu_{\text{Br}} = -0.32$  eV corresponds to Br<sub>2</sub> gas under 300 K and 1 atm. The shaded region indicates the available equilibrium chemical potential region for CsPbBr<sub>3</sub>. Three representative points A ( $\mu_{\text{Br}} = -0.32$  eV,  $\mu_{\text{Pb}} = -2.45$  eV,  $\mu_{\text{Cs}} = -3.68$  eV), B ( $\mu_{\text{Br}} = -0.99$  eV,  $\mu_{\text{Pb}} = -1.22$  eV,  $\mu_{\text{Cs}} = -2.90$  eV), and C ( $\mu_{\text{Br}} = -1.67$  eV,  $\mu_{\text{Pb}} = 0$  eV,  $\mu_{\text{Cs}} = -2.08$  eV) are chosen for calculations of formation energy.

We have considered all possible intrinsic point defects in CsPbBr<sub>3</sub>, namely vacancies ( $V_{\text{Cs}}$ ,  $V_{\text{Pb}}$ ,  $V_{\text{Br}}$ ), interstitials ( $\text{Cs}_i$ ,  $\text{Pb}_i$ ,  $\text{Br}_i$ ), and antisites ( $\text{Cs}_{\text{Pb}}$ ,  $\text{Cs}_{\text{Br}}$ ,  $\text{Pb}_{\text{Br}}$ ,  $\text{Pb}_{\text{Cs}}$ ,  $\text{Br}_{\text{Cs}}$ ,  $\text{Br}_{\text{Pb}}$ ). Three points A, B, and C in Fig. 2 are chosen to calculate the formation energies for the defects. These points represent different growth environments. At point A, the  $\mu_{\text{Br}}$  is close to pure Br<sub>2</sub> gas at 300 K and 1 atm, corresponding to a Br-rich/Pb-poor condition. At point C,  $\mu_{\text{Pb}}$  is close to metal Pb, corresponding to a Br-poor/Pb-rich condition. Point B is in the middle between A and C, thus corresponds to a moderate growth condition. The formation energies of all defects in neutral charge states at these three points are listed in Tab. 1. Under Br-rich condition,  $V_{\text{Cs}}$  has the lowest formation energy of 0.2 eV, therefore it is the dominant defect in this case. The associated intrinsic defect concentration at room temperature, estimated by  $\exp(-\Delta H/k_{\text{B}}T)$ , is  $4 \times 10^{-4}$ . Several other defects also have formation energies less than 1 eV, such as  $V_{\text{Pb}}$ ,  $\text{Br}_i$ ,  $\text{Br}_{\text{Cs}}$ , and  $\text{Cs}_{\text{Pb}}$ . At the B point,

the dominant defect is also  $V_{\text{Cs}}$ , but the formation energy increases to 0.98 eV, and the corresponding concentration decreases to  $10^{-17}$ . Other defects have formation energies larger than 1 eV. Therefore, the overall defect concentration in the moderate condition will be much smaller than that in the Br-rich condition. Under Br-poor condition, the formation energies are all larger than 1 eV. In this case,  $V_{\text{Br}}$  become the dominant defect, with a formation energy of 1.32 eV. The calculated formation energies indicate that Br-rich condition can lead to high defect concentration, and to avoid the formation of defects, the growth should be under moderate or Br-poor condition.

**Table 1: The calculated formation energies (in eV) for neutral defects in  $\text{CsPbBr}_3$  at the three chosen points A, B, and C in Fig. 2.**

	$\text{Cs}_{\text{Br}}$	$\text{Cs}_{\text{i}}$	$\text{Pb}_{\text{i}}$	$\text{Pb}_{\text{Br}}$	$\text{Pb}_{\text{Cs}}$	$V_{\text{Br}}$	$\text{Br}_{\text{Cs}}$	$\text{Br}_{\text{Pb}}$	$\text{Cs}_{\text{Pb}}$	$\text{Br}_{\text{i}}$	$V_{\text{Cs}}$	$V_{\text{Pb}}$
A	6.22	3.55	4.66	6.28	2.44	2.67	0.80	1.40	0.81	0.70	0.20	0.49
B	4.77	2.77	3.44	4.38	1.99	2.00	2.25	3.30	1.26	1.37	0.98	1.71
C	3.27	1.95	2.22	2.48	1.59	1.32	3.75	5.20	1.66	2.05	1.80	2.93

Eq. 2 shows the charge transition level of a given defect. This can be considered as its energy level at different charge states. This level relative to the VBM energy is independent of the chemical potentials of the elements related to the defect. Using HSE+SOC, the transition levels for different charged defect states are calculated, and the results are shown in Fig. 3a. It is seen that only  $\text{Pb}_{\text{Br}}$ ,  $\text{Br}_{\text{Pb}}$ , and  $\text{Pb}_{\text{i}}$  can introduce deep transition levels. All other defects have shallow transition levels, despite that  $\text{CsPbBr}_3$  has a considerable band gap of 2.23 eV. According to Tab. 1, the formation energies of  $\text{Pb}_{\text{Br}}$ ,  $\text{Br}_{\text{Pb}}$ , and  $\text{Pb}_{\text{i}}$  are high, so their concentrations are quite low under all growth conditions. As is known, deep transition levels can act as carrier traps, and result in nonradiative recombination channels. Whereas shallow levels largely preserve the bulk band structure and don't degrade the optoelectronic properties. Our calculations indicate that the formation of deep transition levels in  $\text{CsPbBr}_3$  is difficult, while shallow defects are dominant. In this sense,  $\text{CsPbBr}_3$  is a defect tolerant semiconductor. Synthesizing through simple solution based process can certainly introduce a large amount of defects. Thus the good optoelectronic quality of  $\text{CsPbBr}_3$  is not because

the lack of defects, as some of the defect formation energies are relatively small, rather it is due to its tolerance of such defects.

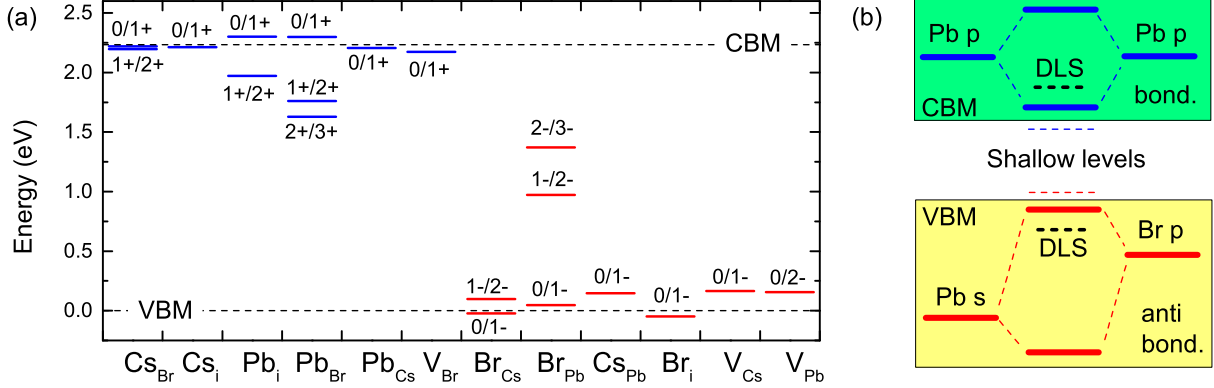


Figure 3: (a) The defect charge transition levels calculated by HSE+SOC. (b) Illustration of the formation of shallow levels.

It will be interesting to understand why the  $\text{CsPbBr}_3$  is defect tolerant. The energy level of the defect can be understood by considering a local picture via the defect localized state (DLS).<sup>31</sup> If the DLS is inside the band gap, the defect is deep. In contrast, if the DLS occurs as a resonance inside the continuum of host bands, it only creates shallow level.<sup>41,42</sup> As discussed above, Cs has no contribution to the band edge states. The top of the valence bands in  $\text{CsPbBr}_3$  originates from the strong  $s$ - $p$  antibonding interaction between Pb and Br. So the VBM is higher than the  $p$  orbital of a Br atom. The empty Pb  $p$  orbitals couple with each other and broaden into the conduction band. So the CBM is lower than the atomic Pb  $p$  orbital. The DLS created by acceptor-like defects in  $\text{CsPbBr}_3$  are Br dangling bond states, which is close to the energy of Br  $p$  orbital. For donor-like defects, DLS are either Pb dangling bond states, which have similar energy with Pb  $p$  orbital, or Cs dangling bond states which are much higher than Pb  $p$  orbital. Hence, all these DLS created by the defects lie either below the VBM or above the CBM, thus result in shallow levels, as illustrated in Fig. 3b. For the cases of these shallow levels (such as  $V_{\text{Br}}(0/1+)$ ), the lattice relaxation of the supercell is not significant compared to the perfect crystal for the  $2 \times 2 \times 2$  supercell we used. Note, all the above arguments hold only when the atomic orbital character (*e.g.*, Pb  $p$ ,

Pb  $s$ , or Br  $p$ ) is either entirely in VBM or CBM, but not both, in other words, the valence band is not coupling with the conduction band. Such feature of the band structure has many consequences. For example, it is found that systems with such band structure feature will not have surface in-gap state for nonpolar surface.<sup>43</sup> Most ionic crystals have such feature, and as a result, the simple ionic vacancy usually does not cause in-gap states, and when the defect is in its proper ionic charge, the Fermi energy will remain in the middle of the band gap.<sup>44</sup> In the cases of  $\text{Pb}_{\text{Br}}$ ,  $\text{Br}_{\text{Pb}}$ , and  $\text{Pb}_i$ , there can be additional bonds such as Pb-Pb and Br-Br. The associated DLS can be shifted down through Pb-Pb bonding or lifted up through Br-Br antibonding interactions, and enter the band gap, leading to the formation of deep levels. For example, in the case of  $\text{Pb}_i^{2+}$  state, the interstitial Pb atom forms Pb-Pb dimer with a host Pb atom, which agrees with previous study on  $\text{CH}_3\text{NH}_3\text{PbI}_3$ .<sup>26</sup> The distance between the Pb atoms in the dimer is 3.91 Å (compared with the Pb-Pb distance of 5.92 Å in perfect crystal). The additional Pb-Pb covalent-bond results in the deep  $\text{Pb}_i(1+/2+)$  level.

In summary, we have studied the formation energies and charge transition levels of all possible intrinsic point defects in  $\text{CsPbBr}_3$ . Under Br-rich and moderate growth condition,  $V_{\text{Cs}}$  is the dominant defect, whereas under Br-poor condition,  $V_{\text{Br}}$  becomes dominant. Moreover, it is found that Br-rich condition can lead to high defect concentration. To avoid the formation of defects, the growth of  $\text{CsPbBr}_3$  should under moderate or Br-poor condition. This does agree with empirical experience in  $\text{CsPbBr}_3$  and the use of excessive Pb during the synthesis.<sup>4</sup> Most of the intrinsic defects induce shallow transition levels, only a few defects with high formation energies can create deep transition levels. Therefore,  $\text{CsPbBr}_3$  is a defect tolerant semiconductor that can keep its qualities despite the presence of defects. Such defect tolerance feature can be attributed to the lacking of bonding-antibonding interaction between the conduction bands and valence bands.

## Acknowledgement

This work was supported by the Director, Office of Science, the Office of Basic Energy Sciences (BES), Materials Sciences and Engineering (MSE) Division of the U.S. Department of Energy (DOE) through the organic/inorganic nanocomposite program (KC3104) under contract DE-AC02-05CH11231. It used resources of the National Energy Research Scientific Computing Center.

## References

- (1) Kojima, A.; Teshima, K.; Shirai, Y.; Miyasaka, T. Organometal Halide Perovskites as Visible-Light Sensitizers for Photovoltaic Cells. *J. Am. Chem. Soc.* **2009**, *131*, 6050–6051.
- (2) Jeon, N. J.; Noh, J. H.; Kim, Y. C.; Yang, W. S.; Ryu, S.; Seok, S. I. Solvent engineering for high-performance inorganic–organic hybrid perovskite solar cells. *Nat. Mater.* **2014**, *13*, 897–903.
- (3) Pan, A.; He, B.; Fan, X.; Liu, Z.; Urban, J. J.; Alivisatos, A. P.; He, L.; Liu, Y. Insight into the Ligand-Mediated Synthesis of Colloidal CsPbBr<sub>3</sub> Perovskite Nanocrystals: The Role of Organic Acid, Base, and Cesium Precursors. *ACS Nano* **2016**, *10*, 7943–7954.
- (4) De Roo, J.; Ibanez, M.; Geiregat, P.; Nedelcu, G.; Walravens, W.; Maes, J.; Martins, J. C.; Van Driessche, I.; Kovalenko, M. V.; Hens, Z. Highly Dynamic Ligand Binding and Light Absorption Coefficient of Cesium Lead Bromide Perovskite Nanocrystals. *ACS Nano* **2016**, *10*, 2071–2081.
- (5) Sun, S.; Yuan, D.; Xu, Y.; Wang, A.; Deng, Z. Ligand-Mediated Synthesis of Shape-Controlled Cesium Lead Halide Perovskite Nanocrystals via Reprecipitation Process at Room Temperature. *ACS Nano* **2016**, *10*, 3648–3657.

- (6) Yang, W. S.; Noh, J. H.; Jeon, N. J.; Kim, Y. C.; Ryu, S.; Seo, J.; Seok, S. I. High-performance photovoltaic perovskite layers fabricated through intramolecular exchange. *Science* **2015**, *348*, 1234–1237.
- (7) Ergen, O.; Gilbert, S. M.; Pham, T.; Turner, S. J.; Tan, M. T. Z.; Worsley, M. A.; Zettl, A. Graded bandgap perovskite solar cells. *Nat. Mater.* **2016**, doi:10.1038/nmat4795.
- (8) Li, G.; Tan, Z.-K.; Di, D.; Lai, M. L.; Jiang, L.; Lim, J. H.-W.; Friend, R. H.; Greenham, N. C. Efficient Light-Emitting Diodes Based on Nanocrystalline Perovskite in a Dielectric Polymer Matrix. *Nano Lett.* **2015**, *15*, 2640–2644.
- (9) Kim, Y.-H.; Cho, H.; Heo, J. H.; Kim, T.-S.; Myoung, N.; Lee, C.-L.; Im, S. H.; Lee, T.-W. Multicolored Organic/Inorganic Hybrid Perovskite Light-Emitting Diodes. *Adv. Mater.* **2015**, *27*, 1248–1254.
- (10) Chen, S.; Roh, K.; Lee, J.; Chong, W. K.; Lu, Y.; Mathews, N.; Sum, T. C.; Nurmiikko, A. A Photonic Crystal Laser from Solution Based Organo-Lead Iodide Perovskite Thin Films. *ACS Nano* **2016**, *10*, 3959–3967.
- (11) Saliba, M. et al. Structured Organic-Inorganic Perovskite toward a Distributed Feedback Laser. *Adv. Mater.* **2016**, *28*, 923–929.
- (12) Zhu, H.; Fu, Y.; Meng, F.; Wu, X.; Gong, Z.; Ding, Q.; Gustafsson, M. V.; Trinh, M. T.; Jin, S.; Zhu, X.-Y. Lead halide perovskite nanowire lasers with low lasing thresholds and high quality factors. *Nat. Mater.* **2015**, *14*, 636–642.
- (13) Dou, L.; Yang, Y. M.; You, J.; Hong, Z.; Chang, W.-H.; Li, G.; Yang, Y. Solution-processed hybrid perovskite photodetectors with high detectivity. *Nat. Commun.* **2014**, *5*, 5404.

- (14) Fang, Y.; Huang, J. Resolving Weak Light of Sub-picowatt per Square Centimeter by Hybrid Perovskite Photodetectors Enabled by Noise Reduction. *Advanced Materials* **2015**, *27*, 2804–2810.
- (15) Protesescu, L.; Yakunin, S.; Bodnarchuk, M. I.; Krieg, F.; Caputo, R.; Hendon, C. H.; Yang, R. X.; Walsh, A.; Kovalenko, M. V. Nanocrystals of Cesium Lead Halide Perovskites ( $\text{CsPbX}_3$ , X = Cl, Br, and I): Novel Optoelectronic Materials Showing Bright Emission with Wide Color Gamut. *Nano Letters* **2015**, *15*, 3692–3696.
- (16) Li, X.; Wu, Y.; Zhang, S.; Cai, B.; Gu, Y.; Song, J.; Zeng, H.  $\text{CsPbX}_3$  Quantum Dots for Lighting and Displays: Room-Temperature Synthesis, Photoluminescence Superiorities, Underlying Origins and White Light-Emitting Diodes. *Adv. Func. Mater.* **2016**, *26*, 2435–2445.
- (17) Bekenstein, Y.; Koscher, B. A.; Eaton, S. W.; Yang, P.; Alivisatos, A. P. Highly Luminescent Colloidal Nanoplates of Perovskite Cesium Lead Halide and Their Oriented Assemblies. *J. Am. Chem. Soc.* **2015**, *137*, 16008–16011.
- (18) Swarnkar, A.; Chulliyil, R.; Ravi, V. K.; Irfanullah, M.; Chowdhury, A.; Nag, A. Colloidal  $\text{CsPbBr}_3$  Perovskite Nanocrystals: Luminescence beyond Traditional Quantum Dots. *Angew. Chem. Int. Ed.* **2015**, *54*, 15424–15428.
- (19) Yettapu, G. R.; Talukdar, D.; Sarkar, S.; Swarnkar, A.; Nag, A.; Ghosh, P.; Mandal, P. Terahertz Conductivity within Colloidal  $\text{CsPbBr}_3$  Perovskite Nanocrystals: Remarkably High Carrier Mobilities and Large Diffusion Lengths. *Nano Lett.* **2016**, *16*, 4838–4848.
- (20) Song, J.; Xu, L.; Li, J.; Xue, J.; Dong, Y.; Li, X.; Zeng, H. Monolayer and Few-Layer All-Inorganic Perovskites as a New Family of Two-Dimensional Semiconductors for Printable Optoelectronic Devices. *Adv. Mater.* **2016**, *28*, 4861–4869.

- (21) Zhang, D.; Eaton, S. W.; Yu, Y.; Dou, L.; Yang, P. Solution-Phase Synthesis of Cesium Lead Halide Perovskite Nanowires. *Journal of the American Chemical Society* **2015**, *137*, 9230–9233.
- (22) Yin, W.-J.; Shi, T.; Yan, Y. Unusual defect physics in  $\text{CH}_3\text{NH}_3\text{PbI}_3$  perovskite solar cell absorber. *Appl. Phys. Lett.* **2014**, *104*, 063903.
- (23) Shi, T.; Yin, W.-J.; Hong, F.; Zhu, K.; Yan, Y. Unipolar self-doping behavior in perovskite  $\text{CH}_3\text{NH}_3\text{PbBr}_3$ . *Appl. Phys. Lett.* **2015**, *106*, 103902.
- (24) Buin, A.; Comin, R.; Xu, J.; Ip, A. H.; Sargent, E. H. Halide-Dependent Electronic Structure of Organolead Perovskite Materials. *Chem. Mater.* **2015**, *27*, 4405–4412.
- (25) Du, M.-H. Density Functional Calculations of Native Defects in  $\text{CH}_3\text{NH}_3\text{PbI}_3$ : Effects of Spin-Orbit Coupling and Self-Interaction Error. *J. Phys. Chem. Lett.* **2015**, *6*, 1461–1466.
- (26) Agiorgousis, M. L.; Sun, Y.-Y.; Zeng, H.; Zhang, S. Strong Covalency-Induced Recombination Centers in Perovskite Solar Cell Material  $\text{CH}_3\text{NH}_3\text{PbI}_3$ . *J. Am. Chem. Soc.* **2014**, *136*, 14570–14575.
- (27) Sebastian, M.; Peters, J. A.; Stoumpos, C. C.; Im, J.; Kostina, S. S.; Liu, Z.; Kanatzidis, M. G.; Freeman, A. J.; Wessels, B. W. Excitonic emissions and above-band-gap luminescence in the single-crystal perovskite semiconductors  $\text{CsPbBr}_3$  and  $\text{CsPbCl}_3$ . *Phys. Rev. B* **2015**, *92*, 235210.
- (28) Shi, H.; Du, M.-H. Shallow halogen vacancies in halide optoelectronic materials. *Phys. Rev. B* **2014**, *90*, 174103.
- (29) Wei, S.-H.; Zhang, S. B. Chemical trends of defect formation and doping limit in II-VI semiconductors: The case of CdTe. *Phys. Rev. B* **2002**, *66*, 155211.

- (30) Zhang, S. B.; Wei, S.-H.; Zunger, A. Intrinsic  $n$ -type versus  $p$ -type doping asymmetry and the defect physics of ZnO. *Phys. Rev. B* **2001**, *63*, 075205.
- (31) Lany, S.; Zunger, A. Assessment of correction methods for the band-gap problem and for finite-size effects in supercell defect calculations: Case studies for ZnO and GaAs. *Phys. Rev. B* **2008**, *78*, 235104.
- (32) Kresse, G.; Hafner, J. Ab initio molecular dynamics for liquid metals. *Phys. Rev. B* **1993**, *47*, 558–561.
- (33) Kresse, G.; Furthmüller, J. Efficient iterative schemes for ab initio total-energy calculations using a plane-wave basis set. *Phys. Rev. B* **1996**, *54*, 11169–11186.
- (34) Kresse, G.; Joubert, D. From ultrasoft pseudopotentials to the projector augmented-wave method. *Phys. Rev. B* **1999**, *59*, 1758–1775.
- (35) Perdew, J. P.; Burke, K.; Ernzerhof, M. Generalized Gradient Approximation Made Simple. *Phys. Rev. Lett.* **1996**, *77*, 3865–3868.
- (36) Heyd, J.; Scuseria, G. E.; Ernzerhof, M. Hybrid functionals based on a screened Coulomb potential. *J. Chem. Phys.* **2003**, *118*, 8207–8215.
- (37) Stoumpos, C. C.; Malliakas, C. D.; Peters, J. A.; Liu, Z.; Sebastian, M.; Im, J.; Chasapis, T. C.; Wibowo, A. C.; Chung, D. Y.; Freeman, A. J.; et al. Crystal Growth of the Perovskite Semiconductor CsPbBr<sub>3</sub>: A New Material for High-Energy Radiation Detection. *Cryst. Growth Des.* **2013**, *13*, 2722–2727.
- (38) Alfe, D. PHON: A program to calculate phonons using the small displacement method. *Comput. Phys. Commun.* **2009**, *180*, 2622 – 2633.
- (39) Paudel, T. R.; Jaswal, S. S.; Tsymbal, E. Y. Intrinsic defects in multiferroic BiFeO<sub>3</sub> and their effect on magnetism. *Phys. Rev. B* **2012**, *85*, 104409.

- (40) Wagman, D. D.; Evans, W. H.; Parker, V. B.; Schumm, R. H.; Halow, I. The NBS tables of chemical thermodynamic properties. Selected values for inorganic and C1 and C2 organic substances in SI units. *J. Phys. Chem. Ref. Data* **1982**, *11*, (Suppl. 2) 50.
- (41) Freysoldt, C.; Grabowski, B.; Hickel, T.; Neugebauer, J.; Kresse, G.; Janotti, A.; Van de Walle, C. G. First-principles calculations for point defects in solids. *Rev. Mod. Phys.* **2014**, *86*, 253–305.
- (42) Zakutayev, A.; Caskey, C. M.; Fioretti, A. N.; Ginley, D. S.; Vidal, J.; Stevanovic, V.; Tea, E.; Lany, S. Defect Tolerant Semiconductors for Solar Energy Conversion. *J. Phys. Chem. Lett.* **2014**, *5*, 1117–1125.
- (43) Zherebetsky, D.; Wang, L.-W. In-Gap States in Electronic Structure of Nonpolar Surfaces of Insulating Metal Oxides. *Adv. Mater. Interfaces* **2014**, *1*, 1300131.
- (44) Zherebetsky, D.; Zhang, Y.; Salmeron, M.; Wang, L.-W. Tolerance of Intrinsic Defects in PbS Quantum Dots. *J. Phys. Chem. Lett.* **2015**, *6*, 4711–4716.